







Structural mechanism underlying primary and secondary coupling between GPCRs and the Gi/o family

Hee Ryung Kim ^{1,6}, Jun Xu^{2,6}, Shoji Maeda ³, Nguyen Minh Duc ^{1,4}, Donghoon Ahn ¹, Yang Du ⁵✉ & Ka Young Chung ¹✉

Heterotrimeric G proteins are categorized into four main families based on their function and sequence, Gs, Gi/o, Gq/11, and G12/13. One receptor can couple to more than one G protein subtype, and the coupling efficiency varies depending on the GPCR-G protein pair. However, the precise mechanism underlying different coupling efficiencies is unknown. Here, we study the structural mechanism underlying primary and secondary Gi/o coupling, using the muscarinic acetylcholine receptor type 2 (M2R) as the primary Gi/o-coupling receptor and the β_2 -adrenergic receptor (β_2 AR, which primarily couples to Gs) as the secondary Gi/o-coupling receptor. Hydrogen/deuterium exchange mass spectrometry and mutagenesis studies reveal that the engagement of the distal C-terminus of G α i/o with the receptor differentiates primary and secondary Gi/o couplings. This study suggests that the conserved hydrophobic residue within the intracellular loop 2 of the receptor (residue 34.51) is not critical for primary Gi/o-coupling; however, it might be important for secondary Gi/o-coupling.

¹School of Pharmacy, Sungkyunkwan University, 2066 Seobu-ro, Jangan-gu, Suwon 16419, Republic of Korea. ²Beijing Advanced Innovation Center for Structural Biology, School of Medicine, Tsinghua University, Beijing 100084, China. ³Department of Molecular and Cellular Physiology, School of Medicine, Stanford University, 279 Campus Drive, Stanford, CA 94305, USA. ⁴Division of Precision Medicine, Research Institute, National Cancer Center, 323 Ilsan-ro, Ilsandong-gu, Goyang 10408, Republic of Korea. ⁵School of Life and Health Sciences, Kobilka Institute of Innovative Drug Discovery, Chinese University of Hong Kong, 2001 Longxiang Ave, Shenzhen, Guangdong 518172, China. ⁶These authors contributed equally: Hee Ryung Kim, Jun Xu. ✉email: yangdu@cuhk.edu.cn; kychung2@skku.edu

G protein-coupled receptors (GPCRs) are the largest receptor superfamily that perceive extracellular signals, including light, smell, taste, hormones, and neurotransmitters¹. Due to their critical functions in physiology and pathology, GPCRs are good therapeutic targets, and one third of approved medicines acts on GPCRs. Thus, it is important to understand the precise signaling mechanism of GPCRs for our fundamental knowledge on the cellular signaling and for the development of better GPCR-targeting therapeutics.

GPCRs propagate extracellular signals into cells by coupling with the heterotrimeric guanine-nucleotide-binding regulatory proteins (G proteins)². The heterotrimeric G proteins are formed by α , β , and γ subunits; in the basal state, $G\alpha$ is occupied by guanosine diphosphate (GDP) and interacts with $G\beta\gamma$ subunits. An agonist-activated receptor interacts with a G protein, which triggers the exchange of GDP for guanosine triphosphate (GTP), followed by dissociation of the $G\alpha$ subunit from the receptor and $G\beta\gamma$ subunits^{2,3}. The GTP-bound $G\alpha$ subunit or $G\beta\gamma$ subunits interact with and regulate downstream effector proteins. Based on their downstream function and sequence, the $G\alpha$ subunits are grouped into four families, G_{as} (G_{as} and $G_{\alpha_{\text{olf}}}$), $G_{\text{ai/o}}$ (G_{ai1} , G_{ai2} , G_{ai3} , G_{ao} , G_{at1} , G_{at2} , G_{at3} , and G_{az}), $G_{\text{aq/11}}$ (G_{aq} , G_{a11} , G_{a14} , and G_{a16}), and $G_{\text{a12/13}}$ (G_{a12} and G_{a13})¹.

Approximately 800 GPCRs have been identified in humans. Previous studies have reported that many GPCRs exhibit promiscuous GPCR-G protein coupling; i.e., a single receptor can interact with more than one G protein subtype^{4–6}. One receptor often couples to more than one $G\alpha$ isoform within the same family due to high sequence similarity⁵. For example, the serotonin 1A receptor interacts with three $G_{\text{i/o}}$ family proteins, G_{i2} , G_{i3} , and G_{o} ⁵. Moreover, several receptors can couple to different G protein families; the α_2 - and β_2 -adrenergic receptors ($\alpha_2\text{AR}$ and $\beta_2\text{AR}$) interact with G_{s} and $G_{\text{i/o}}$ ^{7,8}, the PAR1 receptor with $G_{\text{i/o}}$ and $G_{\text{12/13}}$ ⁹, and the melanin-concentrating hormone receptor 1 with $G_{\text{i/o}}$ and $G_{\text{q/11}}$ ¹⁰.

The interaction efficiency and/or binding kinetics of one receptor to different G proteins often differ. The most prominent coupling, which shows the highest coupling efficiency with fast kinetics, is referred to as ‘primary coupling’. The minor coupling, which shows lower coupling efficiency and/or slower kinetics, is referred to as ‘secondary coupling’^{11,12}. The known primary and secondary GPCR-G protein pairs have been summarized in the IUPHAR/BPS Guide to Pharmacology¹¹ and GPCRdb (gpcrdb.org) (Supplementary Fig. 1a).

Several biochemical/biophysical studies have revealed the conformational dynamics and high-resolution structures of G proteins in various states^{1,3}. These structures of GPCR-G protein complexes reveal the interactions between GPCRs and nucleotide-free G proteins^{13–15}. The X-ray crystal structure of the $\beta_2\text{AR}$ -Gs complex¹⁵ and the cryo-electron microscopy (cryo-EM) structure of the muscarinic acetylcholine receptor type 2-GoA (M2R-GoA) complex¹⁶ are shown in Supplementary Fig. 2. The major binding interface between a receptor and a G protein for both structures is between the C-terminal part of α_5 of the $G\alpha$ subunit and the cytosolic core of the receptor formed by transmembrane domains (Supplementary Fig. 2). The distal C-terminus of $G\alpha$ (the so-called ‘wavy hook’) (Supplementary Fig. 2c, green dotted line)^{17,18} forms an additional α -helical-turn as an extension of α_5 when it interacts with a receptor (Supplementary Fig. 2c). Another interface is the intracellular loop 2 (ICL2) of the receptor interacting with the hydrophobic pocket of $G\alpha$ formed by hydrophobic residues at the $\alpha\text{N}/\beta_1$ hinge, β_2/β_3 loop, and α_5 (Supplementary Fig. 2a, blue dotted box). This interaction appears to be weaker for M2R-GoA structure compared with $\beta_2\text{AR}$ -Gs, which is discussed below.

Recently, using a combination of pulsed hydrogen/deuterium exchange mass spectrometry (HDX-MS), pulsed hydroxyl radical footprinting mass spectrometry (HRF-MS), and mutational studies, we proposed a model that delineates the sequential events during $\beta_2\text{AR}$ -Gs coupling, the primary GPCR-Gs pair¹⁹. In brief, the C-terminal region of G_{as} initially associates with the $\beta_2\text{AR}$ followed by interaction of ICL2 with the hydrophobic pocket within G_{as} , which is the key step for GDP release (see below). Stable helix formation of the G_{as} wavy hook occurs slowly after GDP release.

Although there has been a great progress in understanding the structural mechanism of GPCR-G protein coupling as described above, the structural mechanism of different coupling efficiencies observed from the primary and the secondary coupling has not been clearly elucidated. In the current study, we took advantage of HDX-MS and investigate the structural mechanism that differentiates primary and secondary GPCR-Gi/o coupling using the M2R and the $\beta_2\text{AR}$ as model GPCRs, and G_{i3} and G_{oA} as model Gi/o proteins. The data suggest that the C-terminus of $G_{\text{ai/o}}$ differentiates primary and secondary Gi/o-coupling and that residue 34.51 of the receptor is not important for the primary Gi/o coupling.

Results

M2R- and $\beta_2\text{AR}$ -induced GDP release from Gi/o proteins. The IUPHAR/BPS Guide to Pharmacology¹¹ specifies that the M2R transduces signals primarily through $G_{\text{i/o}}$ family and secondarily through G_{s} and $G_{\text{q/11}}$ families, and the $\beta_2\text{AR}$ transduces signals primarily through G_{s} family and secondarily through $G_{\text{i/o}}$ family (Supplementary Fig. 1b). Especially, the coupling efficiencies of the $\beta_2\text{AR}$ with G_{s} or $G_{\text{i/o}}$ families have been studied extensively both in vitro and in vivo^{20–22}, and the coupling efficiencies of the M2R with G_{s} , $G_{\text{i/o}}$, and $G_{\text{q/11}}$ families have been studied in vivo^{23,24}.

To confirm the different coupling efficiencies of the two different receptors (i.e., primary vs. secondary) for $G_{\text{i/o}}$ proteins, we analyzed receptor-mediated GDP release using purified proteins in vitro. Herein, we used G_{i3} and G_{oA} as model $G_{\text{i/o}}$ proteins (Fig. 1a) as the $\beta_2\text{AR}$ - G_{i3} interaction has been well-characterized in a previous study²¹, and the high-resolution structure of M2R- G_{oA} has been resolved by cryo-EM¹⁶. To achieve optimal $\beta_2\text{AR}$ - $G_{\text{i/o}}$ coupling, we used micelles composed of negatively charged lipids (DDM with POPE at a ratio of 5:1) as the previous study had shown that the charge state of the lipid surrounding the $\beta_2\text{AR}$ affects the efficiency of $G_{\text{i/o}}$ coupling²¹. As expected, the M2R coupled more efficiently to both G_{i3} and G_{oA} than the $\beta_2\text{AR}$, as demonstrated by faster GDP release, with higher efficacy (Fig. 1b) confirming that M2R is primary $G_{\text{i/o}}$ -coupled receptor and $\beta_2\text{AR}$ as secondary $G_{\text{i/o}}$ -coupled receptor. Notably, our previous study showed that the $\beta_2\text{AR}$ induced almost complete GDP release from G_{s} within 10 s¹⁹, confirming that the $\beta_2\text{AR}$ primarily couples to G_{s} .

M2R- or $\beta_2\text{AR}$ -induced HDX profile changes in GaoA. Previously, we analyzed the conformational differences between GDP-bound G_{as} and $\beta_2\text{AR}$ -bound nucleotide-free G_{as} using HDX-MS²⁵; HDX levels near the nucleotide-binding pocket were higher in $\beta_2\text{AR}$ -bound nucleotide-free G_{as} than in GDP-bound G_{as} , which reflects GDP release and increased structural dynamics in this region (Supplementary Fig. 3). The C-terminal part of α_5 of G_{as} displayed a lower HDX level in $\beta_2\text{AR}$ -bound nucleotide-free G_{as} than in the GDP-bound G_{as} (Supplementary Fig. 3) reflecting a stable helix formation and insertion into the receptor cytosolic core (described in Supplementary Fig. 2c).

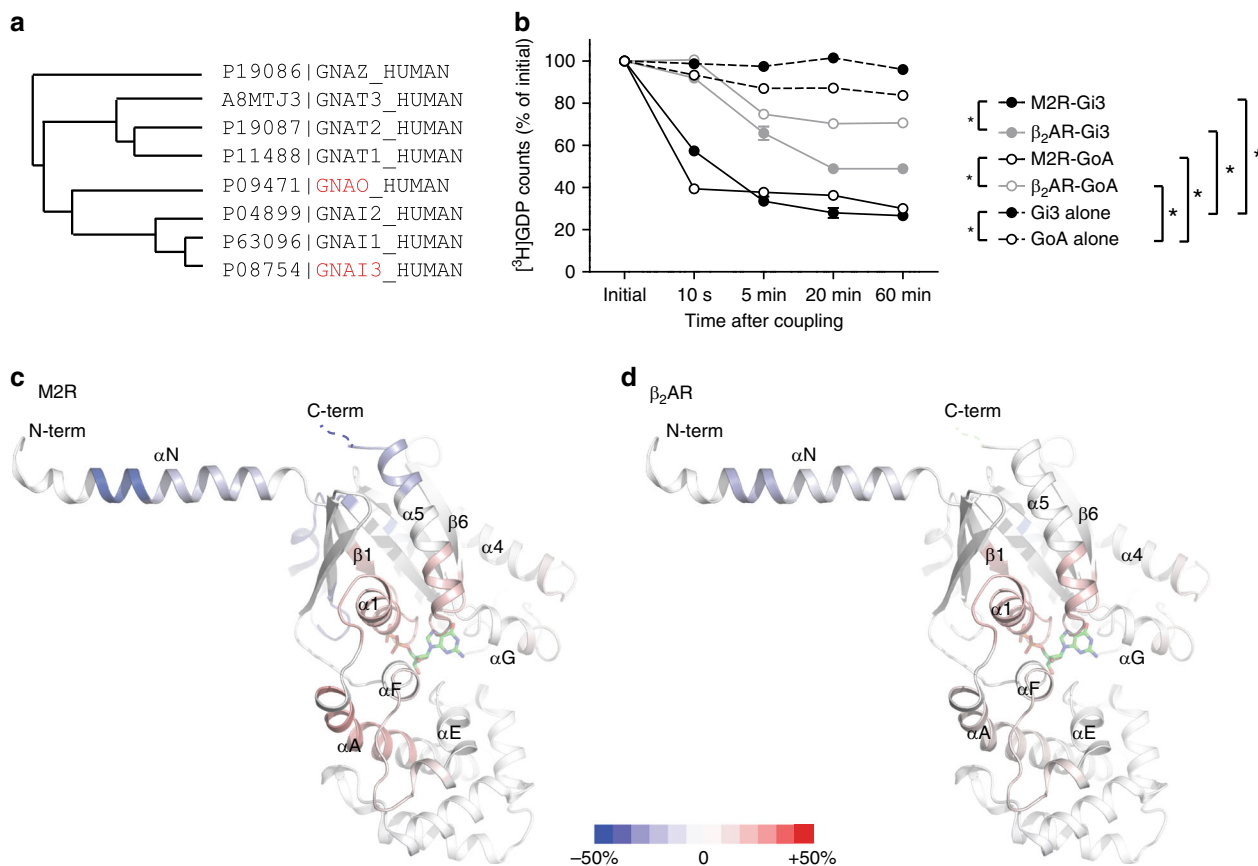


Fig. 1 GDP release and HDX-MS analysis of different GPCR-G protein pairs. **a** Phylogenetic tree of Gαi/o families. The phylogenetic tree is generated based on the protein sequences provided by UNIPROT database (uniprot.org). The uniprot ID is indicated in front of the protein names. **b** GDP release profiles of GoA and Gi3, induced by the M2R or the β₂AR. * Indicates statistical differences between groups analyzed by one-way ANOVA test ($p < 0.05$). Error bars represent mean \pm S.E.M. of three independent experiments. Source data are provided as a Source data file. **c, d** HDX level changes of GαoA after 3 h of incubation with the M2R (**c**) or the β₂AR (**d**). The changes in HDX are color-coded on the X-ray crystal structure of Gαi1 (PDB 1GP2). The deuterium uptake plots are provided in Supplementary Fig. 4a.

To understand the structural mechanism of different GDP release efficiencies between M2R-Gi/o and β₂AR-Gi/o pairs, here we analyzed HDX levels of GαoA in GDP-bound GoA heterotrimer alone and in GoA heterotrimer after M2R or β₂AR co-incubation (Fig. 1c, d and Supplementary Fig. 4a). The co-incubation of GoA with the M2R or the β₂AR did not affect HDX profiles of Gβγ subunits (Supplementary data) implying that Gβγ subunits do not undergo significant conformational changes upon complex formation with the M2R or the β₂AR. When GoA was incubated with its primary coupling receptor M2R, we detected decreased HDX at the C-terminal part of α5 (Fig. 1c and Supplementary Fig. 4a, peptides 341–348 and 349–353), which suggests decreased dynamics and/or exclusion from the buffer. We detected increased HDX near the nucleotide binding pocket (Fig. 1c and Supplementary Fig. 4a, peptides 37–52, 268–275, and 324–333), which suggests GDP release and/or increased dynamics. We also detected increased HDX between Ras-like and α-helical domains (Fig. 1c and Supplementary Fig. 4a, peptides 53–61, 276–285, and 289–298) and a few peptides from the α-helical domain (AHD) (Fig. 1c and Supplementary Fig. 4b, peptides 65–77 and 161–173), which could be attributed to domain opening and dynamic movement of AHD²⁶. These results are consistent with those of the previous HDX-MS study that analyzed β₂AR-Gs complex (Supplementary Fig. 3a)²⁵. We detected decreased HDX at αN (Fig. 1c and Supplementary Fig. 4a, peptides 14–18 and 19–29), which was not detected in β₂AR-Gs complex due to lack of identified peptides in this region;

the decreased HDX at αN may reflect the interaction of this region with the M2R (Supplementary Fig. 2b) and/or the blockage of this region from the buffer by micelles surrounding the receptor.

When GoA was incubated with the β₂AR, a secondary coupling receptor, the HDX profile changes were similar in most regions except the C-terminal part of α5 (Fig. 1c, d). For instance, we detected increased HDX near the nucleotide-binding pocket and AHD, and decreased HDX at αN, although to a lesser extent than the M2R-GoA pair (Fig. 1d and Supplementary Fig. 4a). However, surprisingly, the C-terminal part of GαoA did not show HDX profile changes (Fig. 1d and Supplementary Fig. 4a, peptides 341–342 and 349–353), which implies that the C-terminal part of GαoA may not form the stable helix upon β₂AR-GoA coupling and/or may not be deeply inserted into the receptor core.

Time-resolved HDX during M2R- and β₂AR-Gi/o coupling.

The HDX profile changes shown in Fig. 1 are comparisons between before and after 3 h of co-incubation of GoA with the receptors. Three hours of co-incubation of the receptor and GoA is sufficient for completion of GDP release and formation of the final receptor-GoA complex^{16,21}. Therefore, the data in Fig. 1 do not reflect transient conformational changes during coupling.

Recently, we performed HDX-MS in a pulsed manner to gain insight into time-resolved conformational changes during primary

GPCR-Gs coupling using β_2 AR-Gs pair as model system¹⁹. In this previous study, the β_2 AR and Gs were sampled before co-incubation, and after 10 s, 5 min, 20 min, 60 min, 90 min, 110 min, 150 min, and 180 min of co-incubation. The sampled proteins were then pulsed with deuterated buffer for 10 or 100 s¹⁹. This approach provides the HDX profiles of the indicated time points, which reflect the conformational states of the β_2 AR and Gs at the sampled time points (Supplementary Fig. 5a). Pulsed HDX-MS analysis of β_2 AR-Gs revealed HDX profile change at ICL2 of the β_2 AR within 10 s of co-incubation (Supplementary Fig. 5a, peptides 133–144) whereas the HDX profile change continued until 110 min at the N-terminal part of ICL3 (Supplementary Fig. 5a, peptide 223–240), which suggests that ICL2 undergoes conformational changes faster than ICL3 upon coupling to Gs. Analysis of Gas detected rapid HDX profile changes at the nucleotide-binding pocket (Supplementary Fig. 5a, peptides 49–59 and 367–371) and slow and prolonged HDX profile changes at the C-terminus of $\alpha 5$ (Supplementary Fig. 5a, peptide 382–390)¹⁹. We confirmed that GDP release occurs within 10 s of co-incubation with the β_2 AR indicating that the rapid HDX profile changes at the nucleotide-binding pocket was mainly due to GDP release¹⁹. Interestingly, the prolonged HDX profile changes at the C-terminus of $\alpha 5$ suggested that this region undergoes prolonged conformational changes even after GDP release¹⁹.

In the current study, we adopted the same strategy to investigate whether the C-terminal part of Gai/o does ever form a stable helix and/or is inserted into the receptor cytosolic core, during the time-course of β_2 AR-Gi/o coupling (Fig. 2 and Supplementary Fig. 5b). We used 10 s deuterium pulse for M2R-Gi/o coupling and 10 and 100 s deuterium pulses for β_2 AR-Gi/o coupling because 10 s deuterium pulse was not sufficient to observe HDX differences between Gi/o alone and Gi/o co-incubated with the β_2 AR, for a few peptides (for example, peptides 37–52, 53–61, 268–275, and 324–333 in Supplementary Fig. 4a). Again, we did not detect any HDX profile changes of G $\beta\gamma$ subunits during the co-incubation time course (Supplementary data).

When GoA or Gi3 was co-incubated with the M2R, the HDX profile change at αN was initiated within 10 s and completed within 10 s to 5 min (peptides 14–18 and 19–29 for GaoA in Fig. 2 and peptides 6–18 and 19–33 for Gai3 in Supplementary Fig. 5b). The HDX profile changes of αN showed similar results when Gi3 or GoA was incubated with the β_2 AR (Fig. 2 and Supplementary Fig. 5b). However, the previous study with the β_2 AR and Gs reported that HDX profile at αN of Gas increased within 10 s of incubation with the β_2 AR (Supplementary Fig. 5a) suggesting that the conformational changes at αN may differ between GPCR-Gs and GPCR-Gi/o coupling.

The HDX profile change near the nucleotide-binding pocket was initiated within 10 s and completed within 5–20 min in M2R-Gi3/GoA pairs (peptides 37–52 and 324–333 for GaoA in Fig. 2 and peptides 37–52 and 324–334 for Gai3 in Supplementary Fig. 5b). Interestingly, GDP release was completed within 10 s to 5 min for M2R-Gi/o coupling (Fig. 1b), which was faster than the changes in HDX-MS profile near the nucleotide-binding pocket. This may reflect further conformational changes after GDP release; the initial HDX profile changes within 10 s to 5 min were due to GDP release, while the later HDX profile changes observed at 20 min were due to additional conformational changes after GDP release. However, we cannot exclude the possibility that these discrepancies between GDP release and HDX-MS profile change kinetics could also be due to different experimental conditions between the two assay systems such as protein concentration (see the Methods for details).

When Gi3 or GoA was incubated with the β_2 AR, the HDX profile changes near the nucleotide-binding pocket were initiated

within 10 s and completed within 10 s to 5 min, which was faster than M2R-Gi3/GoA pairs (Fig. 2 and Supplementary Fig. 5b). The GDP release was initiated within 5 min and completed within 20 min of co-incubation of the β_2 AR and Gi3/GoA (Fig. 1b), and the discrepancies between GDP release and HDX-MS profile change kinetics could be due to different experimental conditions between the two assay systems; the coupling may be slower in the GDP release assay probably due to lower protein concentrations. Overall, it is tempting to propose that the nucleotide-binding pocket undergoes further conformational changes after GDP release in M2R-Gi3/GoA coupling whereas the conformational changes near the nucleotide-binding pocket in β_2 AR-Gi3/GoA pairs are smaller and quicker probably due to the lack of further conformational changes after GDP release.

The HDX profile of the C-terminal part of GaoA continued to decrease until 150–180 min during M2R-GoA coupling (Fig. 2, peptides 342–348 and 349–353), which is similar to what we observed with β_2 AR-Gs coupling¹⁹ (Supplementary Fig. 5a, peptides 382–390). On the other hands, during M2R-Gi3 coupling, the HDX profile change at the C-terminal part of Gai3 was initiated within 10 s and continued to decrease until 20 min (Supplementary Fig. 5b, peptides 342–348 and 349–353). The molecular mechanism underlying the different HDX profile change kinetics at the C-terminal part of GaoA and Gai3 needs further investigation. Interestingly, when incubated with the β_2 AR, the C-terminal part of GaoA or Gai3 never showed decreased HDX at any time point during coupling (Fig. 2 and Supplementary Fig. 5b).

In summary, the M2R-induced HDX profile changes in GaoA or Gai3 were similar to what we observed for the β_2 AR-induced HDX profile changes in Gas except at the αN . However, β_2 AR-Gi/o complex showed no HDX-MS profile change at the C-terminal part of Gai/o, which implied that this region of Gai/o does not form stable helices during β_2 AR-Gi/o coupling and/or may not be deeply inserted into the cytoplasmic core of the receptor.

The role of the wavy hook for Gi/o coupling. As the C-terminal part of Gai/o displayed the most differences in HDX-MS profiles between M2R-Gi/o and β_2 AR-Gi/o coupling, we hypothesized that the C-terminal part of Gai/o differentiates between primary and secondary GPCR-Gi/o coupling.

The C-terminal part of Ga that we analyzed with HDX-MS can be divided into two parts; one is the distal C-terminus (Fig. 3a, green-colored residues, ‘wavy hook’), and the other is the C-terminal helical region of $\alpha 5$ (Fig. 3a, black residues). In our previous study with the β_2 AR and Gs, we observed that the C-terminal part of Ga is the initial site that undergoes a change in hydroxyl radical foot printing upon interaction with the β_2 AR¹⁹. Moreover, the β_2 AR failed to induce GDP release from the wavy hook-truncated Gas, which suggested that the wavy hook is the critical initial binding site during β_2 AR-Gs coupling¹⁹ (see below).

To test the role of the wavy hook in GPCR-Gi/o coupling, we also generated a Gai3 mutant construct in which the last five residues were truncated (hereafter denoted Gi3 Δ 5). Unlike β_2 AR-Gs coupling, both the M2R and the β_2 AR could induce GDP release from Gi3 Δ 5 (Fig. 3b). Interestingly, β_2 AR-induced GDP release profile did not change upon C-terminal truncation, while M2R-induced GDP release was decreased so that the extent of this GDP release became similar between β_2 AR-Gi3, β_2 AR-Gi3 Δ 5, and M2R-Gi3 Δ 5 (Fig. 3b). These data suggest that the wavy hook of Gai3 has a role in differentiating between primary and secondary coupling; it is likely that the engagement of the wavy hook of Gai3 with a receptor is necessary for primary

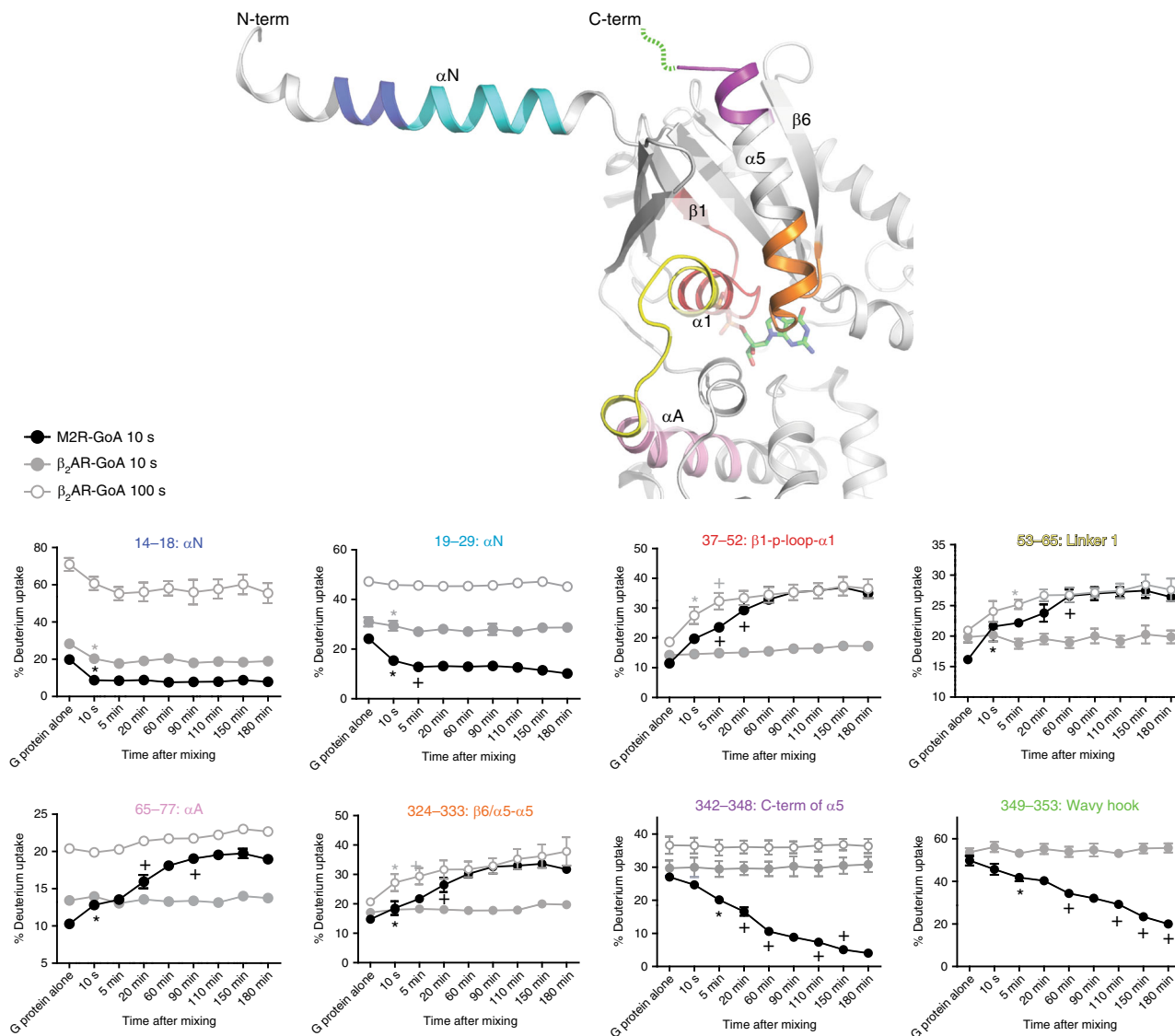


Fig. 2 Time-resolved HDX profiles of G α oA during M2R-GoA and β_2 AR-GoA coupling. The selected analyzed peptides are color-coded on the X-ray crystal structure of G α i1 (PDB 1GP2) and on the titles of deuterium uptake graphs. Statistically significant changes during coupling were analyzed by repeated-measures ANOVA (rANOVA). To compare two different time points, a two-tailed paired Student's t-test was performed, and $p < 0.05$ was considered as statistically significant. * Indicates the first time point that showed a statistical difference compared with before co-incubation. + Indicates the first time point that showed a statistical difference from previously marked (either * or +) time point. Error bars represent mean \pm S.E.M of three independent experiments. Please note that the data is plotted using a non-linear/non-logarithmic scale.

(i.e., strong) coupling, while failure in doing so (evident from HDX-MS studies of β_2 AR-Gi/o coupling or from GDP release analysis of M2-Gi3_Δ5 coupling) leads to secondary (i.e., weak) coupling.

The role of the wavy hook for GPCR-Gi/o coupling selectivity.

As Gi3_Δ5 could still couple with receptors (Fig. 3b), we hypothesized that truncation of the wavy hook of Gi3 results in loss of coupling selectivity and leads to promiscuous coupling with non-Gi/o-coupling receptors. To test this hypothesis, we analyzed the GDP release activity of the M1R on WT Gi3 and Gi3_Δ5. According to the IUPHAR/BPS Guide to Pharmacology and a previous report, the M1R primarily couples with Gq/11²⁴ (Supplementary Fig. 1b), and we confirmed that the M1R does not couple with WT Gi3 (Fig. 3c). However, we clearly observed M1R-induced GDP release from Gi3_Δ5, although the coupling efficiency was low (approximately 20% GDP release) (Fig. 3c). These data support our hypothesis that

truncation of the distal C-terminus of Gi3 induces promiscuous coupling with non-Gi/o-coupling receptors.

The potential mechanism of promiscuous coupling of Gi3_Δ5 with the M1R may be attributed to its higher intrinsic dynamics relative to WT Gi3. In other words, the wavy hook may assist in retaining Gi3 in the GDP-bound state. However, we did not detect any difference in basal GDP release between WT Gi3 and Gi3_Δ5 (Fig. 3c). To further investigate the basal GDP/GTP exchange tendency, we analyzed the uptake of BODIPY-conjugated GTPγS (BODIPY-GTPγS) into WT Gai3 and Gai3_Δ5. We used the α subunit of Gi3—without forming a heterotrimer with G $\beta\gamma$ —to facilitate GDP/GTP turnover (Fig. 3d, e). The BODIPY fluorescence increases when BODIPY-GTPγS is located within the nucleotide-binding pocket compared with when it is free in the buffer allowing the detection of GTPγS binding by measuring the BODIPY fluorescence^{27,28}. BODIPY-GTPγS binding to WT Gai3 and Gai3_Δ5 occurred with similar kinetics (Fig. 3d), although the maximal binding was slightly

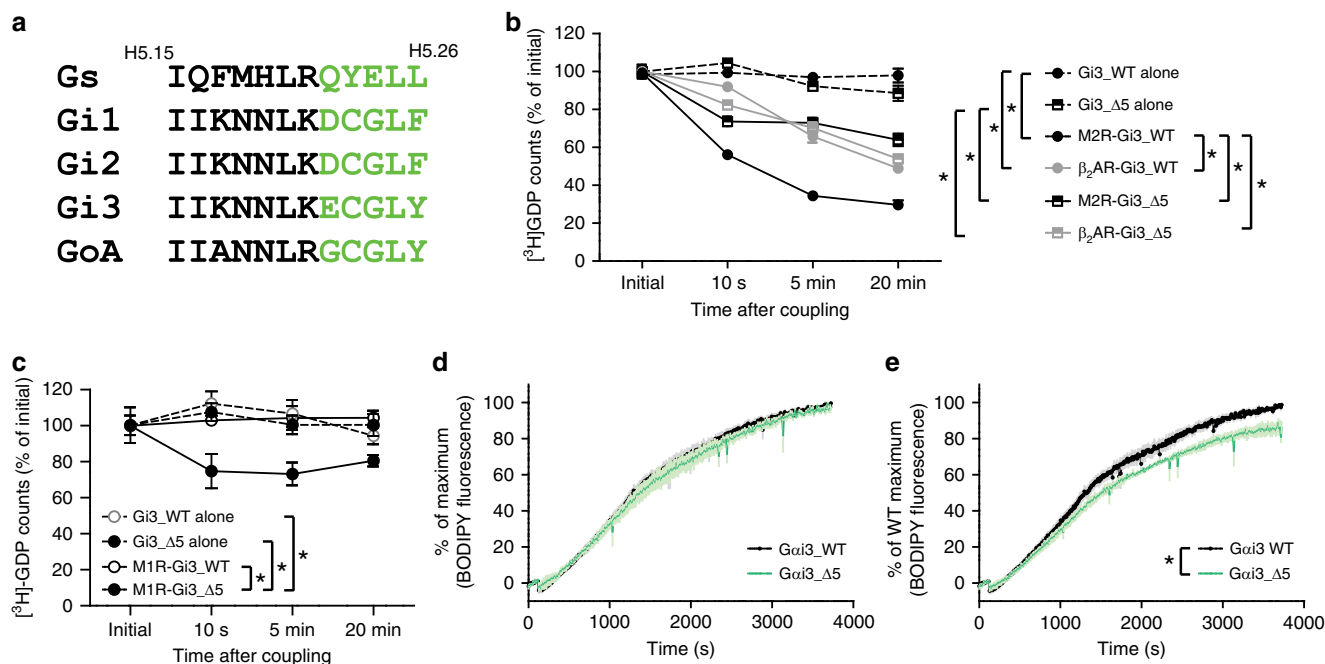


Fig. 3 The role of $G\alpha i3$ wavy hook in primary and secondary Gi coupling. **a** Sequence alignment of the C-terminal part of $G\alpha s$ and $G\alpha i/o$ proteins. **b** GDP release profiles of $Gi3_WT$ and $Gi3_Δ5$ induced by the M2R or the β_2AR . **c** GDP release profiles of $Gi3_WT$ and $Gi3_Δ5$ induced by the M1R. For **(b)** and **(c)**, * indicates statistical differences between groups analyzed by one-way ANOVA test ($p < 0.05$). Error bars represent mean \pm S.E.M. of at least three independent experiments ($n = 3-6$). **d** BODIPY fluorescence presented as percent (%) of maximum of each sample. **e** BODIPY fluorescence presented as percent (%) of WT $G\alpha i3$ maximum. Error bars (gray for WT $G\alpha i3$ and light green for $G\alpha i3_Δ5$) represent mean \pm S.E.M. of three independent experiments. * Indicates statistical differences between groups analyzed by a two-tailed Student's t test ($p < 0.05$). Source data are provided as a Source data file.

higher in WT $G\alpha i3$ than that in $G\alpha i3_Δ5$ (Fig. 3e). These data suggest that the intrinsic GDP release activity of $G\alpha i3_Δ5$ is not higher than that of WT $G\alpha i3$, and therefore M1R-induced GDP release from $Gi3_Δ5$ is not due to increased intrinsic GDP release activity.

Gi/o-induced HDX profile changes of M2R and β_2AR . To gain more insights into the structural changes that occur upon receptor-Gi/o coupling, we compared the HDX levels of the M2R and the β_2AR before and after 3 h of co-incubation with GoA (Fig. 4a, b, and Supplementary Fig. 4b) and analyzed the time-resolved HDX changes in the M2R and the β_2AR during M2R-Gi/o and β_2AR -Gi/o coupling (Fig. 4c).

As discussed above, we have previously analyzed the HDX profile changes in the β_2AR upon co-incubation with Gs, and observed decreased HDX at ICL2 and the N-terminal region of ICL3 of the β_2AR (Supplementary Fig. 5a)¹⁹. The decreased HDX at ICL2 reflects helix formation and interaction of F139 with the hydrophobic pocket of Gs (as shown in Supplementary Fig. 2a, blue dotted box), and the decreased HDX at the N-terminus of ICL3 reflects extended helix formation upon interaction with the C-terminal part of Gs (as shown in Supplementary Fig. 2a, green square).

We could not identify peptides from ICL2 region of the M2R but could analyze the N-terminal region of ICL3. Unlike the β_2AR -Gs complex, this region did not undergo HDX changes (Fig. 4a). This is consistent with the high-resolution structures of the M2R, where the N-terminal region of ICL3 does not form an extended helix upon interaction with GoA (Supplementary Fig. 4c). Helix 8 (H8) of the M2R showed decreased HDX (Fig. 4a and Supplementary Fig. 4b), which may be caused by the interaction between H8 and the C-terminal part of $G\alpha i/o$, as observed in the high-resolution structures of GPCR-Gi/o complexes¹⁷. Unfortunately, we could not obtain the pulsed

HDX-MS data from H8, and therefore we could not correlate the time-course of conformational changes between the C-terminal part of $G\alpha i/o$ and M2R H8.

For the β_2AR -Gi/o complex, when we compared the HDX profiles before and after 3 h of co-incubation of the β_2AR with GoA, HDX levels on the β_2AR were not altered at any of the analyzed regions (Fig. 4b). A time-resolved HDX-MS study also showed that the N-terminal region of ICL3 of the β_2AR does not undergo decreased HDX at any of the tested timepoints during coupling with $Gi3$ (Fig. 4c, peptides 223-240). A lack of HDX change at the N-terminus of ICL3 suggests that the β_2AR fails to form extended helices at the N-terminal region of ICL3 when coupled with Gi/o. This observation is consistent with the lack of HDX change at the C-terminal part of GaoA or $G\alpha i3$ (Fig. 1d, Fig. 2, and Supplementary Fig. 5b), which strengthens the hypothesis that the C-terminus of GaoA or $G\alpha i3$ is not deeply inserted into the β_2AR core.

However, time-resolved analysis of HDX profile change showed that the HDX level at ICL2 underwent a transient decrease (within 10 s of co-incubation) upon co-incubation with $Gi3$ (Fig. 4c, peptides 133-144). After 10 s, the HDX level was not statistically different either from the 10 s time point or from the point of β_2AR alone. These results suggest that ICL2 engages with $Gi3$ during an early event, but that the interaction may not be stable.

Importance of ICL2 in primary and secondary Gi/o coupling.

Our previous studies suggested that for β_2AR -Gs coupling, the interaction of a bulky hydrophobic residue, F139 at ICL2, (residue 34.51, based on GPCRdb numbering scheme) with the hydrophobic pocket formed by H41, V217, F219, and F376 (Supplementary Fig. 2a) is the critical step to induce GDP release^{19,29}. For example, mutation of Phe139 to Ala in the β_2AR (hereafter denoted β_2AR_F139A) abolished β_2AR -induced GDP release from Gs, although this construct could still interact with Gs¹⁹. On

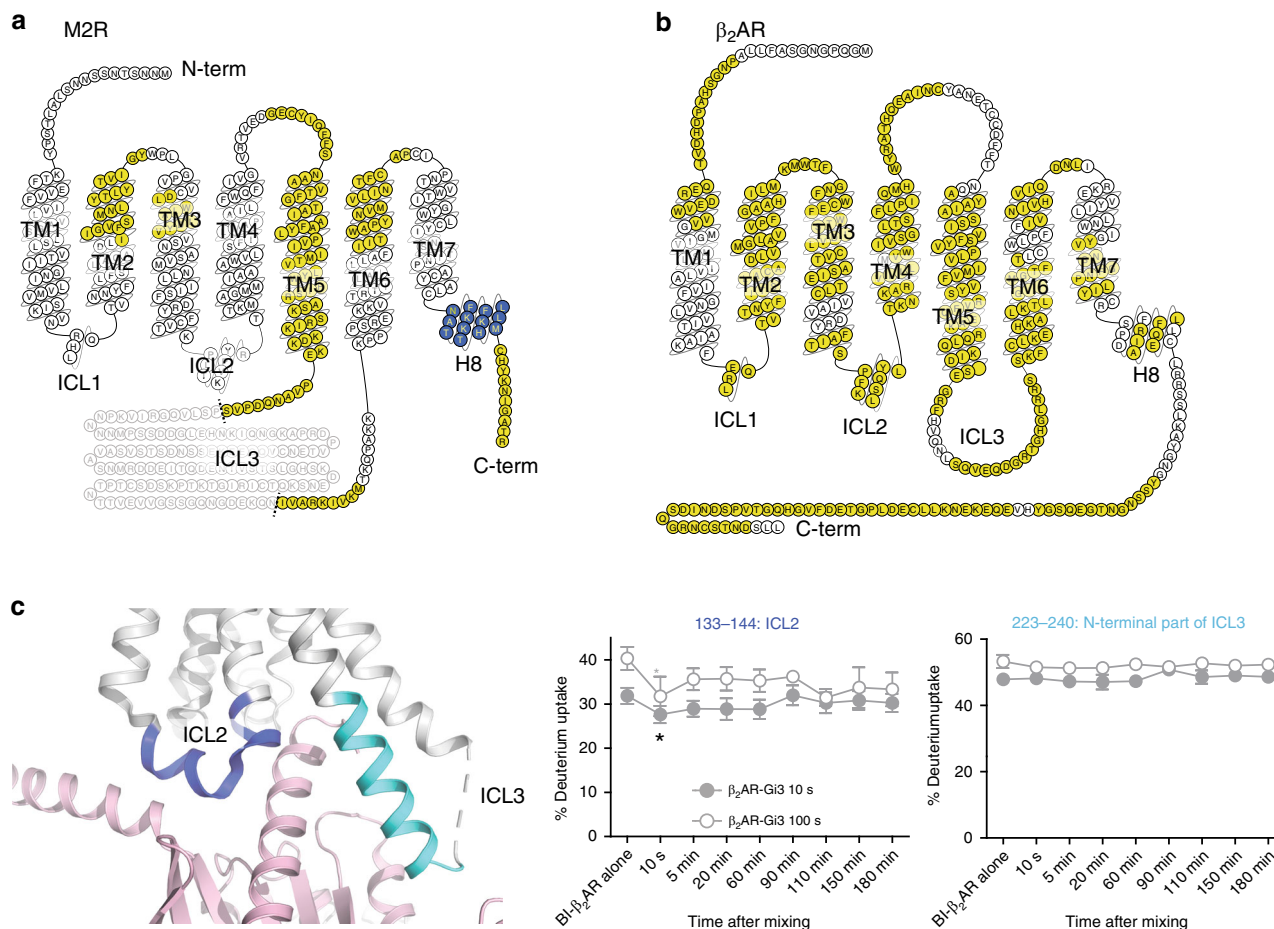


Fig. 4 HDX profiles of the receptors during M2R-GoA and β_2 AR-GoA coupling. **a, b** HDX level changes of the M2R (**a**) and the β_2 AR (**b**) after 3 h of incubation with GoA. The changes in HDX are color-coded on the snake maps from GPCRdb (gpcrdb.org). Gray residues in M2R indicate truncated ICL3 for better expression and purification. White residues indicate regions without identified peptides; yellow residues indicate regions without HDX changes; and blue residues indicate regions with decreased HDX upon co-incubation with GoA. **c** Pulsed HDX-MS analysis of selected peptides of the β_2 AR during β_2 AR-Gi/o coupling. The selected peptides analyzed are color-coded on the X-ray crystal structure of β_2 AR (PDB 3SN6) and on the titles of the deuterium uptake graphs. Light pink color represents G α_s . Statistically significant changes during coupling were analyzed by repeated-measures ANOVA (rANOVA). To compare two different time points, a two-tailed paired Student's *t*-test was performed, and *p* < 0.05 was considered as statistically significant. * Indicates the first time point that showed a statistical difference compared with pre-incubation experiments. Please note that the data is plotted using a non-linear/non-logarithmic scale.

the other hands, the currently available high-resolution structures of GPCR-Gi/o complexes show that hydrophobic residues at 34.51 form weak hydrophobic interactions with the hydrophobic pocket formed by V34, L194/L195, F196/F197, and F336 of the Gai/o families (Fig. 5a).

To test the role of the interaction of residue 34.51 in primary and secondary GPCR-Gi coupling, we generated mutant constructs in which the bulky hydrophobic residue at 34.51 was replaced with Ala (M2R_L129A and β_2 AR_F139A). M2R_L129A could still induce GDP release from Gi3, albeit to a lesser degree than WT M2R (Fig. 5b). This result is consistent with the previous report in which M2R_L129A induced GDP/GTP turnover, although the degree was reduced to 50% relative to that in WT M2R¹⁶. Unlike M2R_L129A-Gi3 coupling, β_2 AR_F139A failed to release GDP from Gi3 (Fig. 5c), which suggests that the bulky hydrophobic residue 34.51 at ICL2 is critical for β_2 AR-Gi3 coupling.

To gain more insights into the role of residue 34.51 in GPCR-Gi/o coupling, we analyzed the amino acid residue at position 34.51 in class A GPCRs with known coupling G proteins (Supplementary Fig. 1 and Fig. 5d-f). Among the Gs-coupled

receptors, 26% contain Phe or Tyr, and 68% contain large hydrophobic residues such as Ile, Leu, or Met (Fig. 5d). Thus, a majority (94%) of Gs-coupled receptors comprise of very large/large hydrophobic or aromatic ring-containing amino acid residues at position 34.51. Similarly, a majority (82%) of Gq/11-coupled receptors contain very large/large hydrophobic or aromatic ring-containing amino acid residues at position 34.51 (Fig. 5d). In contrast, the proportion of very large/large hydrophobic or aromatic ring-containing amino acid residues at position 34.51 decreases in Gi/o-coupled receptors (56%), while the proportion of medium or small hydrophobic amino acids at position 34.51 increases in Gi/o-coupled receptors (25.3%) (Fig. 5d). Moreover, 17.7% of Gi/o-coupled receptors contain non-hydrophobic residues (His, Pro, Ser, Thr, Arg, Lys, Glu, and Gln) whereas only 4.5% of Gs-coupled receptors and 13.1% of Gq/11-coupled receptors contain these residues (Fig. 5d). These sequence analyses imply that the bulky hydrophobic residue at 34.51 is important for Gs or Gq/11 coupling, but this may not be necessarily true for Gi/o coupling.

We further analyzed amino acids at position 34.51 of all class A Gi/o-coupled receptors (Fig. 5e). Comparison of the

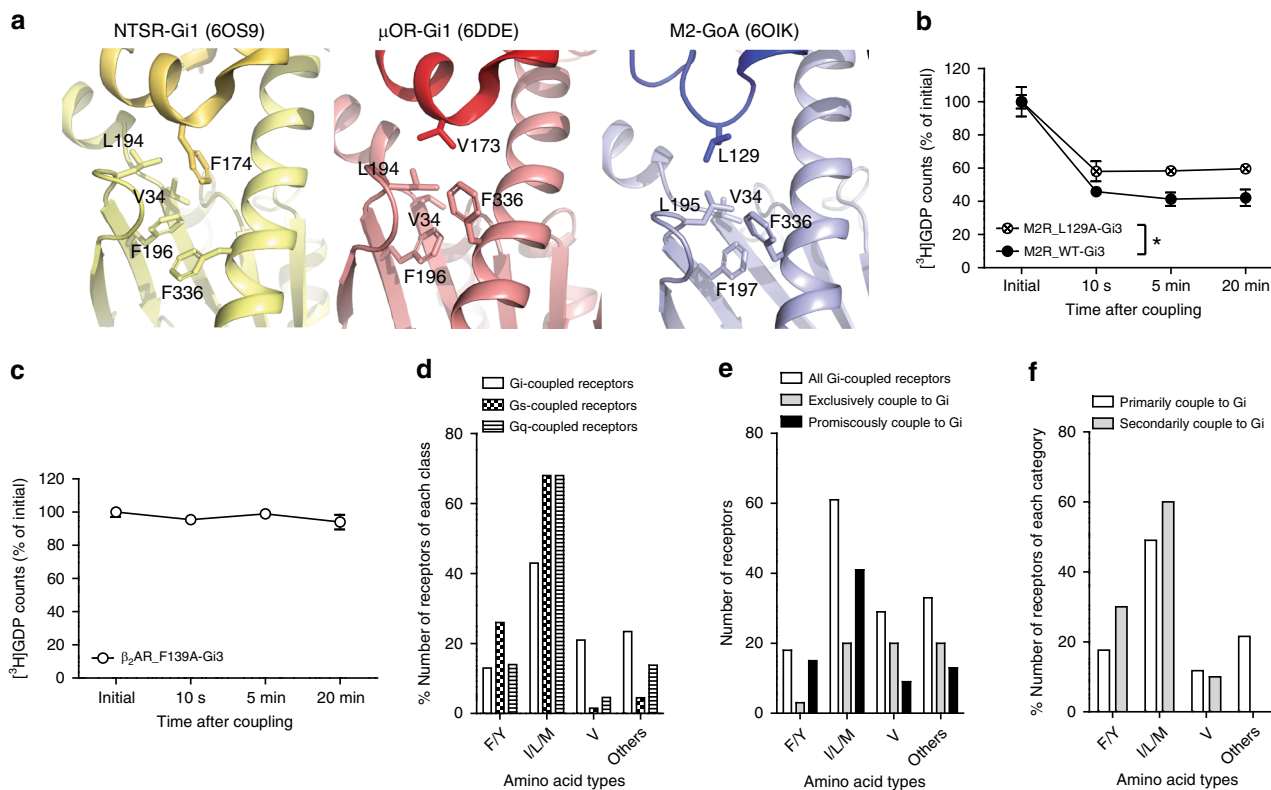


Fig. 5 The role of residue 34.51 within ICL2 in M2R-Gi3 and $\beta_2\text{AR}$ -Gi3 coupling. **a** The structures of ICL2 and hydrophobic pocket of neurotensin receptor-Gi1 complex (left, PDB 6OS9), mu-opioid receptor-Gi1 complex (middle, PDB 6DDE), and M2R-GoA complex (right, PDB 6OIK). Receptors are shown in dark color, and G proteins are shown in light color. **b** GDP release profiles of M2R-Gi3 and M2R_L129A-Gi3. **c** GDP release profiles of $\beta_2\text{AR}_\text{F139A}$ -Gi3. For **(b)** and **(c)**, * indicates statistical differences between groups as analyzed by a two-tailed Student's *t*-test ($p < 0.05$). Error bars represent mean \pm S.E.M of three independent experiments. Please note that the data is plotted using a non-linear/non-logarithmic scale. **d** Amino acid type analysis at residue 34.51 of type A GPCRs with known coupling G proteins. **e** Amino acid type analysis at residue 34.51 of type A Gi/o-coupled receptors subcategorized into exclusive or promiscuous coupling. **f** Amino acid type analysis at residue 34.51 of promiscuously Gi/o-coupled receptors, which are subcategorized into primary and secondary coupling. Source data are provided as a Source data file.

exclusively-Gi/o-coupled and promiscuously-Gi/o-coupled receptors revealed a broad range of amino acid residues in the exclusively-Gi/o-coupled receptors contain, whereas the promiscuously-Gi/o-coupled receptors contain mostly very large/large hydrophobic or aromatic ring-containing amino acid residues (56 receptors out of 78 promiscuously-Gi/o-coupled receptors) (Fig. 5e). When we further subcategorized the promiscuously-Gi/o-coupled receptors into primarily-Gi/o-coupled receptors and secondarily-Gi/o-coupled receptors, we found that all the receptors that secondarily couple to Gi/o contain Phe/Tyr, Ile/Leu/Met, or Val and do not contain other amino acids while the receptors that primarily couple to Gi/o contain these amino acids as well as other residues such as Ala, His, Pro, Ser/Thr, Arg/Lys, and Gln (Fig. 5f). These findings imply that for the secondary GPCR-Gi/o interaction, the bulky hydrophobic residue at ICL2 may be important, which is consistent with the observation that $\beta_2\text{AR}_\text{F139A}$ failed to release GDP from Gi3 (Fig. 5c).

Taken together, we suggest that the interaction of residue 34.51 with the hydrophobic pocket within the $\text{G}\alpha$ subunit is not critical for primary GPCR-Gi/o coupling, but it is important for secondary GPCR-Gi/o coupling.

Discussion

Previous studies have suggested that a single receptor differentially activates different G proteins to varying degrees and/or with different kinetics, which results in complex signal transduction^{6,9,30}. This fine-tuning of GPCR-G protein coupling is important for the

precise regulation of cellular functions. However, only few studies have suggested the mechanism underlying differential coupling of promiscuous receptors; for example, the availability of G proteins limits the GPCR-G protein coupling selectivity^{4,7}, and different ligand types or ligand concentrations differentially regulate the promiscuity of GPCR-G protein coupling^{31,32}.

The current study presents the conformational factors that differentiate between primary and secondary Gi/o-coupling. We found that one of the key structural factors is the engagement of the wavy hook of $\text{G}\alpha$ with the receptor (Fig. 6b vs. Fig. 6c). Failure of strong engagement of the wavy hook with the receptor leads to secondary Gi/o coupling (i.e., $\beta_2\text{AR}$ -Gi/o, $\beta_2\text{AR}$ -Gi3_Δ5, or M2R-Gi3_Δ5).

These results are surprising because the engagement of the distal C-terminus of $\text{G}\alpha$ with receptors has been considered to be critical for GPCR-G protein interaction and coupling selectivity^{19,20,33–39}. In our previous study using the $\beta_2\text{AR}$ and Gs, truncation of the wavy hook resulted in the complete loss of $\beta_2\text{AR}$ -induced GDP release, and we suggested that the wavy hook is the initial binding site¹⁹ (Fig. 6a). However, the present data indicate that the M2R and the $\beta_2\text{AR}$ could still couple to the 'wavy hook-truncated' $\text{G}\alpha$ 3 (Fig. 3b), and moreover, the M1R, a non-Gi/o-coupled receptor, can induce GDP release from Gi3_Δ5 but not from WT Gi3 (Fig. 3c). It is tempting to suggest that the wavy hook of Gi3 facilitates interaction with primary Gi/o-coupled receptors but inhibits interaction with non-Gi/o-coupled receptors (Fig. 6d). The detailed molecular mechanism of the role of the wavy hook in differentiating primary vs. secondary Gi/o-coupling and preventing interaction with the

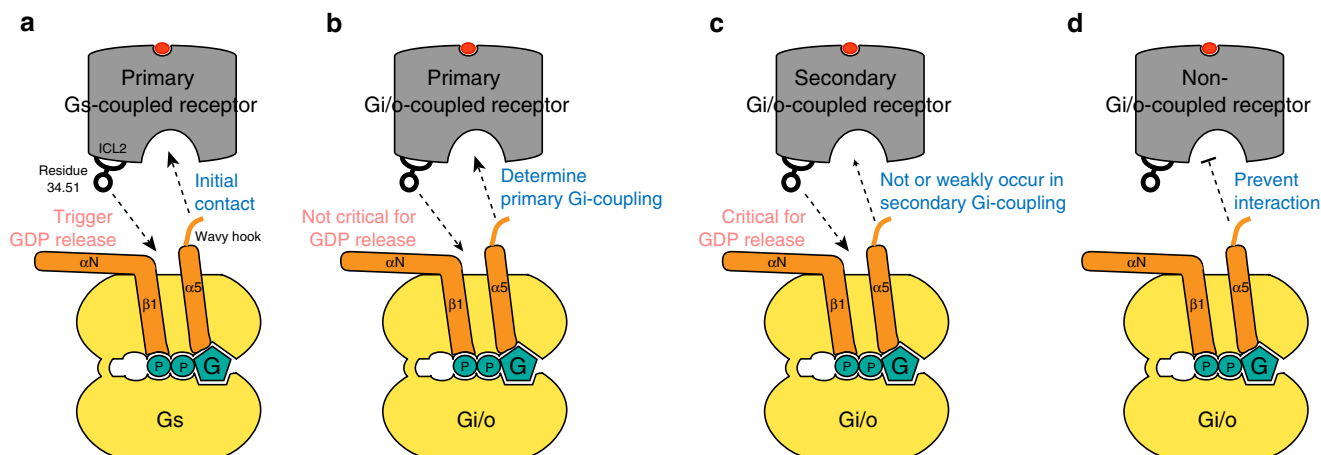


Fig. 6 Summary of Gs and Gi/o coupling mechanisms. **a** The structural mechanism of primary Gs-coupling based on the study by Du et al.¹⁹ is illustrated. Wavy hook is the initial contact site with a receptor followed by interaction of residue 34.51 at ICL2 with $G\alpha_s$, which triggers GDP release. **b, c** The structural mechanism of primary and secondary Gi/o-coupling is illustrated. Interaction of the wavy hook with the receptor determines primary and secondary Gi/o coupling. Interaction of residue 34.51 at ICL2 with $G\alpha_i/o$ is critical for secondary Gi/o-coupling but not for primary Gi/o-coupling. **d** The wavy hook of $G\alpha_i/o$ prevents coupling with non-Gi/o-coupled receptors.

non-Gi/o-coupled receptors needs further investigation using systematic mutagenesis or swap mutation of the wavy hook.

Different coupling modes between primary and secondary Gi/o-coupling were also found at receptor residue 34.51 (Fig. 6b vs. Fig. 6c) as the bulky hydrophobic residue at 34.51 is critical for β_2AR -Gi3 coupling but not for M2R-Gi3 coupling (Fig. 5b, c). Previous studies reported that residue 34.51 within ICL2 of the receptor is critical for receptor-G protein coupling^{19,40}. Interestingly, the importance of residue 34.51 has been mostly observed for GPCR-Gs interaction^{19,40} but not for GPCR-Gi/o interaction (Supplementary Fig. 2a vs. Fig. 5a). The analysis of the amino acid type at residue 34.51 supports the hypothesis that the bulky hydrophobic residue at 34.51 is important for primary GPCR-Gs or GPCR-Gq/11 coupling, but may not be critical for primary GPCR-Gi/o coupling (Fig. 5). Interestingly, all the receptors that secondarily couple to Gi/o contain large hydrophobic amino acids at residue 34.51 (Fig. 5f) suggesting that such amino acids at position 34.51 may be necessary for secondary GPCR-Gi/o coupling.

The current study also suggests that primary Gi/o coupling might follow certain different structural mechanisms compared with primary Gs coupling (Fig. 6a vs Fig. 6b). First, αN showed increased HDX in β_2AR -Gs coupling and decreased HDX in M2R-Gi3/GoA coupling (Fig. 2 and Supplementary Fig. 5). Second, the β_2AR failed to induce GDP release from $Gs_{\Delta 5}$ ¹⁹, but the M2R still induced GDP release from $Gi3_{\Delta 5}$ (Fig. 3b). Third, β_2AR_{F139A} failed to induce GDP release from Gs ¹⁹, but M2R_{L129A} still induced GDP release from Gi3 (Fig. 5b). These discrepancies may provide clues to understand GPCR-G protein selectivity, which needs further investigation.

In conclusion, we propose the potential conformational mechanism differentiating primary and secondary Gi/o-coupling and compared the conformational mechanism of primary Gi/o-coupling with that of primary Gs-coupling. The findings raise questions about the detailed functional mechanism of the wavy hook in facilitating primary Gi/o coupling and preventing non-Gi/o coupling. Moreover, the critical step for GDP release during primary GPCR-Gi/o coupling is remained to be elucidated because the interaction of the residue 34.51 was not critical for GPCR-Gi/o coupling as suggested in GPCR-Gs coupling.

Methods

Expression and purification of Gi/o. Following protocol is for expression and purification of samples used for Figs. 1, 2, 4, and 5. Human GaoA or Gai3 was

cloned into pFastBac1 vector; G β 1 with 3C protease-cleavable 6xHis-tag and G γ 2 were cloned into pFastBac_Dual vector. The G proteins were expressed in High Five insect cells (Expression Systems, 94-001F) using Bac-to-Bac system. Cell cultures were grown at 27 °C to a density of 3×10^6 cells mL⁻¹ and then infected with Gao or Gai3 and G β 1 γ 2 baculovirus (10–20 mL L⁻¹ and 1–2 mL L⁻¹ respectively). After 48 h incubation, the infected cells were harvested by centrifugation and stored at –80 °C until use. Cell pellets were resuspended in 100 mL lysis buffer (10 mM Tris, pH 7.5, 0.1 mM MgCl₂, 5 mM β -mercaptoethanol (β -ME), 10 μ M GDP, 2.5 μ g mL⁻¹ leupeptin, and 160 μ g mL⁻¹ benzamidine) per liter of culture volume and stirred at room temperature for 15 min. Cell membranes were then spun down and resuspended in 100 mL solubilization buffer (20 mM HEPES, pH 7.5, 100 mM NaCl, 1% sodium cholate, 0.05% DDM, 5 mM MgCl₂, 2 μ L CIP, 5 mM β -ME, 15 mM imidazole, 10 μ M GDP, 2.5 μ g mL⁻¹ leupeptin, and 160 μ g mL⁻¹ benzamidine) per liter of culture volume using a Dounce homogenizer. The sample were stirred at 4 °C for 1 h, and then centrifuged for 20 min to remove insoluble debris. Nickel-NTA resin (2 mL L⁻¹ cell culture) pre-equilibrated in solubilization buffer was added to the supernatant and shaken for 2 h at 4 °C. After incubation, the Ni-NTA resin was spun down, poured into a glass column, and washed with 50 mL solubilization buffer. The heterotrimeric GoA or Gi3 was then gradually exchanged into E2 buffer (20 mM HEPES pH 7.5, 50 mM NaCl, 0.1 % DDM, 1 mM MgCl₂, 5 mM β -ME, 10 μ M GDP, 2.5 μ g mL⁻¹ leupeptin, and 160 μ g mL⁻¹ benzamidine). The protein was then eluted with E2 buffer supplemented with 250 mM imidazole. The protein was then dephosphorylated by treating with 5 μ L lambda phosphatase (supplemented with 1 mM MnCl₂ for activity), 1 μ L CIP, and 1 μ L Antarctic phosphatase, then incubated at 4 °C overnight. The 6xHis-tag was removed using 3C protease. Cleaved GoA or Gi3 was purified by an additional negative Ni-NTA purification step. The Ni-NTA chromatography purified GoA or Gi3 was further purified with MonoQ column (GE Healthcare). The peak fractions of MonoQ column were collected and concentrated using a 50 kDa molecular weight cutoff Millipore concentrator. The concentrated heterotrimeric GoA or Gi3 was aliquoted, flash frozen in liquid nitrogen and frozen at –80 °C before use.

Expression and purification of WT and mutant $G\alpha i3_{\Delta 5}$. Following protocol is for expression and purification of samples used for Fig. 3. The recombinant Gai/o protein containing N-terminal His-tag and TEV cleavage site was constructed in pET21a. Gai3_Δ5 mutant was generated by site-directed mutagenesis using PCR. The primers used for mutagenesis are listed in Supplementary Table 1. Gai3 and Gai3_Δ5 were transformed into *Escherichia coli* LOBST (Kerfast, EC1002) and GaoA was transformed into *Escherichia coli* BL21-DE3 (iNTRON, ITY-YE207). Cells were grown in Terrific Broth in the presence of antibiotic at 37 °C until OD₆₀₀ reached 0.6–0.8. Protein expression was induced by 0.03 mM IPTG and cells were further incubated at 16 °C for 24 h. For protein purification, the cell pellets were harvested and resuspended in lysis buffer (20 mM HEPES pH 7.4, 300 mM NaCl, 2 mM MgCl₂, 20 μ M GDP, 1:1000 protease inhibitor cocktail, 2.5 μ g mL⁻¹ leupeptin, 10 μ g mL⁻¹ benzamidine, 100 μ M TCEP, and 10% glycerol) in three folds of cell pellet volume and incubated with 5 mg mL⁻¹ lysozyme for 30 min at room temperature. The lysate was then incubated with 10 μ g mL⁻¹ DNaseI for another 30 min. The supernatant was collected by centrifugation at 20,000 \times g for 30 min at 4 °C, supplemented with 20 mM imidazole, and loaded onto Ni-NTA column equilibrated with lysis buffer containing 20 mM imidazole. The Ni-NTA resin was washed with wash buffer (20 mM HEPES pH 7.4, 300 mM NaCl, 2 mM MgCl₂,

20 μM GDP, 1:1000 protease inhibitor cocktail, 2.5 $\mu\text{g mL}^{-1}$ leupeptin, 10 $\mu\text{g mL}^{-1}$ benzamide, 100 μM TCEP, and 20 mM imidazole. The proteins were eluted with elution buffer (20 mM HEPES pH 7.4, 300 mM NaCl, 2 mM MgCl_2 , 20 μM GDP, 1:1000 protease inhibitor cocktail, 2.5 $\mu\text{g mL}^{-1}$ leupeptin, 10 $\mu\text{g mL}^{-1}$ benzamide, 100 μM TCEP, and 250 mM imidazole). Proteins were further purified using a Superdex-200 (10/300) column with ÄKTA FPLC. The protein fractions were collected by monitoring the absorbance at 280 nm. Proteins were then concentrated, supplemented with 20% glycerol, and stored at -80°C until further use.

Expression and purification of the M2R and the M1R. Human M2R and M1R genes, containing N-terminal FLAG-tag and C-terminal His-tag, were subcloned into pFastBac1 vector. The L129A mutation of M2R was generated by Quick-Change mutagenesis and confirmed by DNA sequencing. The primers used for mutagenesis are listed in Supplementary Table 1. All M2R and M1R constructs used in this study were expressed in Sf9 insect cells (Expression Systems, 94-002F) using the Bac-to-Bac baculovirus system. Sf9 cells were grown in the ESF 921 medium and were infected with recombinant baculovirus at a density of 4×10^6 cells mL^{-1} , in the presence of 10 μM atropine. The cells were harvested after 48 h of infection at 27°C . Cell pellets were lysed using a lysis buffer (10 mM Tris pH 7.5, 1 mM EDTA, 10 μM atropine, 2.5 $\mu\text{g mL}^{-1}$ leupeptin, and 160 $\mu\text{g mL}^{-1}$ benzamide). Cell membranes were then spun down and solubilized with a buffer containing 20 mM HEPES (pH 7.5), 750 mM NaCl, 1% DDM, 0.2% sodium cholate, 0.03% CHS, 10 μM atropine, 2.5 $\mu\text{g mL}^{-1}$ leupeptin, 160 $\mu\text{g mL}^{-1}$ benzamide, and 30% glycerol. The solubilized receptor was then purified through Ni-NTA chromatography and eluted with a buffer containing 20 mM HEPES (pH 7.5), 750 mM NaCl, 0.1% DDM, 0.02% sodium cholate, 0.03% CHS, 10 μM atropine, and 30% glycerol and supplemented with 250 mM imidazole. The Ni-NTA purified receptor was then loaded onto an anti-FLAG column with M1 affinity resin and washed extensively with a buffer containing 20 mM HEPES (pH 7.5), 750 mM NaCl, 0.1% DDM, 0.02% sodium cholate, 0.003% CHS, and 10 μM iperoxo and supplemented with 2 mM CaCl_2 . Thereafter, it was eluted with the same buffer supplemented with 0.2 mg mL^{-1} of FLAG peptide and 5 mM of EDTA. The anti-FLAG-chromatography-purified receptor was finally purified by size exclusion chromatography against a buffer containing 20 mM HEPES (pH 7.5), 100 mM NaCl, 0.1% DDM, 0.003% CHS, and 10 μM iperoxo. The monodisperse peak fractions were concentrated, flash frozen, and stored at -80°C until further use.

Expression and purification of the $\beta_2\text{AR}$. The $\beta_2\text{AR}$ was expressed in Sf9 insect cells (Expression Systems, 94-002F) using the BestBac expression system. The F139A mutation was generated by Quick-Change mutagenesis and confirmed by DNA sequencing. The primers used for mutagenesis are listed in Supplementary Table 1. Proteins were expressed by infecting Sf9 cells at 4×10^6 cells mL^{-1} with second-passage baculovirus using 20 mL L^{-1} of cell culture supplemented with 2 μM alprenolol. The cells were harvested after 48 h incubation at 27°C . Cell pellets were resuspended in lysis buffer (20 mM HEPES pH 7.5, 5 mM EDTA, 1 μM alprenolol, 2.5 $\mu\text{g mL}^{-1}$ leupeptin, and 160 $\mu\text{g mL}^{-1}$ benzamide) at 10 mL g^{-1} of cell pellet and stirred for 15 min. The collected cell membrane was then homogenized by a Douncer device with the sample in solubilization buffer (20 mM HEPES, pH 7.5, 100 mM NaCl, 1% DDM, 1 μM alprenolol, 2.5 $\mu\text{g mL}^{-1}$ leupeptin, and 160 $\mu\text{g mL}^{-1}$ benzamide) for 1 h at room temperature to extract the receptor. After adding 2 mM CaCl_2 , the supernatant was collected by centrifugation at 18,000 $\times g$ for 30 min and loaded onto anti-FLAG column with M1-antibody resin. The column was thoroughly washed with HMS-CHS buffer (20 mM HEPES pH 7.5, 350 mM NaCl, 0.1% DDM, and 0.01% cholesterol hemisuccinate) supplemented with 2 mM CaCl_2 . The receptor was then eluted with HMS-CHS buffer supplemented with 5 mM EDTA and 200 $\mu\text{g mL}^{-1}$ FLAG peptide. The eluted protein was kept frozen and thawed immediately prior to use. The thawed receptor was further purified via alprenolol-Sepharose affinity chromatography using HMS-CHS buffer with 300 μM alprenolol as the elution buffer. The eluted receptors were once again loaded onto anti-FLAG column and washed with HMS-CHS buffer to achieve unliganded receptors by removing alprenolol. The bound receptor was then eluted with HMS-CHS buffer with 5 mM EDTA, 200 $\mu\text{g mL}^{-1}$ FLAG peptide and 10 μM BI-167107. The functional receptors were further purified by size exclusion chromatography using a Superdex-200 column in HLS-CHS buffer 20 mM HEPES pH 7.5, 150 mM NaCl, 0.1% DDM, 0.01% CHS, 2 μM BI-167107. The receptors were concentrated, flash frozen in liquid nitrogen, and stored at -80°C until use.

GPCR-Gi/o complex formation and HDX-MS. To form GPCR-Gi/o complex, Gi/o (65 μM) was mixed with 1.15-fold molar excess of iperoxo-bound M2R or BI-167107-bound $\beta_2\text{AR}$ at room temperature. Apyrase (200 mU mL^{-1}) was added after 90 min of incubation to hydrolyze GDP, and to generate a stable complex. For continuous labeling deuterium exchange, 5 μL of complex, agonist bound receptor or GDP-bound Gi/o was mixed with 25 μL of D_2O buffer (20 mM HEPES (pH 7.4), 100 mM NaCl, 100 mM TCEP, and 0.1% DDM) supplemented with 5 μM agonist, 20 μM GDP, or both for receptor alone, G protein alone, or complex, respectively) and incubated for 10, 100, 1000, and 10,000 s at room temperature. For pulse-labeling deuterium exchange, GPCR and Gi/o were mixed at room temperature as described above, and 5 μL aliquots were collected at the indicated time points

(before mixing, 10 s, 5 min, 20 min, 60 min, 90 min, 110 min, 150 min, and 180 min), mixed with 25 μL of D_2O buffer, and incubated for 10 s or 100 s at room temperature. The deuterated samples were quenched using 30 μL of ice-cold quench buffer (0.1 M NaH_2PO_4 and 20 mM TCEP (pH 2.01)), snap-frozen on dry ice, and stored at -80°C . Non-deuterated samples were prepared by mixing 5 μL of protein sample with 25 μL of their respective H_2O buffers, followed by quenching and freezing, as described above.

The quenched samples were digested and isolated using the HDX-UPLC-ESI-MS system (Waters, Milford, MA, USA). Briefly the quenched samples were thawed and immediately injected into an immobilized pepsin column (2.1 \times 30 mm) (Life Technologies, Carlsbad, CA, USA) at a flow rate of 100 $\mu\text{L min}^{-1}$ in 0.05% formic acid in H_2O at 12°C . The peptic peptides were then collected on a C18 VanGuard trap column (1.7 $\mu\text{m} \times$ 30 mm) (Waters) for desalting with 0.05% formic in H_2O and subsequently separated by ultra-pressure liquid chromatography using an Acquity UPLC C18 column (1.7 μm , 1.0 \times 100 mm) (Waters) at a flow rate of 40 $\mu\text{L min}^{-1}$ with an acetonitrile gradient starting from 8 to 85% over 8.5 min using two pumps. The mobile phase A was 0.1% formic acid in H_2O and the mobile phase B was 0.1% formic acid in acetonitrile. Buffers were adjusted to pH 2.5 and the system was maintained at 0.5°C (except pepsin digestion was performed at 12°C) to minimize the back-exchange of deuterium to hydrogen. Mass spectra were analyzed by Xevo G2 quadrupole-time of flight (Q-TOF) equipped with a standard electrospray ionization (ESI) source in MS^E mode (Waters) with positive ion mode. The capillary, cone, and extraction cone voltages were set to 3 kV, 40 V, and 4 V, respectively. Source and desolvation temperatures were set to 120°C and 350°C , respectively. Trap and transfer collision energies were set to 6 V, and the trap gas flow was set to 0.3 mL min^{-1} . The mass spectrometer was calibrated with sodium iodide solution (2 $\mu\text{g mL}^{-1}$). [Glu1]-Fibrinopeptide B solution (200 $\mu\text{g mL}^{-1}$) in MeOH:water (50:50 (v/v) + 1% acetic acid) was utilized for the lock-mass correction and the ions at mass-to-charge ration (m/z) 785.8427 were monitored at scan time 0.1 s with a mass window of ± 0.5 Da. The reference internal calibrant was introduced at a flow rate of 20 $\mu\text{L min}^{-1}$ using the lock mass sprayer and the acquired spectra were automatically corrected using the lock-mass. Two independent interleaved acquisitions were automatically created: the first function, typically set at 4 eV, collected low energy or unfragmented data while the second function collected high energy or fragmented data typically obtained by using a collision ramp from 30–55 eV. Ar gas was used for collision induced dissociation (CID). Mass spectral were acquired in the range of m/z 100–2000 for 10 min. ProteinLynx Global Server 2.4 (Waters) was utilized to identify peptic peptides from the non-deuterated samples with variable methionine oxidation modification and a peptide score of 6. DynamX 2.0 software (Waters) was used to determine the level of deuterium uptake for each peptide by measuring the centroid of isotopic distribution. The average back-exchange in our system was ~30–40%, but we did not correct for back exchange because the proteins aggregate in fully deuterated samples. All the data were derived from at least three independent experiments. The detailed HDX-MS results are summarized in the supplementary data, which were generated according to Masson et al.'s recommendation⁴¹.

GDP release assay. Purified G α subunit (200 nM) of each G protein (Go α or Gi3) was mixed with 50 nM of [³H]GDP for 1 h at room temperature, in a buffer containing 20 mM HEPES (pH 7.5), 100 mM NaCl, 0.1% DDM, 100 μM TCEP, and 2 μM GDP. Thereafter, 2 μM of purified G $\beta\gamma$ was added. After 10 min of incubation, 5 μM of BI-167107-bound $\beta_2\text{AR}$, iperoxo-bound M2R, or the corresponding DDM buffer, of similar volume, was further added to initiate GDP release, in the presence of 1 μM GDP. The reaction mixture was aliquoted at indicated time points, and immediately loaded onto calibrated G-50 columns. The flow through was collected with 1.1 mL of buffer (20 mM HEPES (pH 7.5), 100 mM NaCl, and 0.1% DDM), and Go α - or Gi3-bound [³H]GDP was measured using a scintillation counter (Beckman Coulter, Brea, CA, USA), after adding 15 mL of scintillation fluid. The initial sample represents [³H]GDP binding capacity of Go α or Gi3, before initiation of GDP release.

BODIPY-GTP γ S assay. Nucleotide binding to GaoA and Gai3 were determined by measuring change in fluorescence intensity of BODIPY-FL-GTP γ S (Thermo Fisher Scientific, Waltham, MA, USA) in an imaging buffer comprised of 20 mM Tris-HCl (pH 8.0), 1 mM EDTA, 10 mM MgCl_2 , and 100 μM TCEP. The fluorophore was excited at 485 nm (bandwidth 14 nm) and the emission spectrum was recorded at 535 nm (bandwidth 25 nm) using TriStar2 S LB 942 Multimode Microplate Reader (Berthold, Germany). Baseline in absence of protein samples was determined by measuring fluorescence intensity of imaging buffer with or without 50 nM BODIPY-FL-GTP γ S for 120 s. GaoA and Gai3 prepared in 20 mM HEPES (pH 7.4), 100 mM NaCl, 2 mM MgCl_2 , 100 μM TCEP, and 10 μM GDP were mixed with imaging buffer with or without 50 nM BODIPY-FL-GTP γ S in 1:10 dilution (1.5 μM final GaoA and Gai3 concentration). The changes in fluorescence were measured for 60 min. Data points were collected every 10 s using a 96-well black plate. All steps were carried out at room temperature. The spectra were corrected by measurements in absence of BODIPY-FL-GTP γ S and normalized by setting the peak fluorescence of BODIPY-FL-GTP γ S in presence of protein as 100.

Statistics and reproducibility. Results are representatives of at least three independent experiments and are expressed as mean \pm S.E.M. Statistical analysis was performed using GraphPad Prism software (San Diego, CA, USA). Statistical significance of time-dependent changes was determined by repeated-measures one-way ANOVA (rANOVA) at a level = 0.01 followed by Turkey's multiple comparison test; change in a time series as a whole was considered significant when the F statistic was >1 . The significance of differences between two different time points within series or two groups was determined by paired or unpaired two-tailed Student's *t*-test. The significance of differences between more than two groups was determined by one-way ANOVA. Analysis was considered significant at $p < 0.05$.

Reporting summary. Further information on research design is available in the Nature Research Reporting Summary linked to this article.

Data availability

Data supporting the findings of this manuscript are available from the corresponding authors upon reasonable request. A reporting summary for this Article is available as a Supplementary Information file.

HDX-MS data have been deposited to ProteomeXchange Consortium⁴² via PRIDE⁴³ partner repository with the set identifier PXD019367. The source data underlying Figs. 1b, 3b–e, and 5b–f are provided as a Source Data file. Data for sequence analysis in Fig. 5d–f are available from GPCR database (gpcrdb.org).

Received: 4 February 2020; Accepted: 4 June 2020;

Published online: 22 June 2020

References

- Syrovatkina, V., Alegre, K. O., Dey, R. & Huang, X. Y. Regulation, signaling, and physiological functions of G-proteins. *J. Mol. Biol.* **428**, 3850–3868 (2016).
- Milligan, G. & Kostenis, E. Heterotrimeric G-proteins: a short history. *Br. J. Pharm.* **147**, S46–S55 (2006).
- Mahoney, J. P. & Sunahara, R. K. Mechanistic insights into GPCR-G protein interactions. *Curr. Opin. Struct. Biol.* **41**, 247–254 (2016).
- Milligan, G. Is promiscuity of G protein interaction an issue in the classification of receptors? *Ann. N. Y. Acad. Sci.* **812**, 126–132 (1997).
- Albert, P. R. & Robillard, L. G protein specificity: traffic direction required. *Cell Signal* **14**, 407–418 (2002).
- Woehler, A. & Ponomasov, E. G. G protein-mediated signaling: same receptor, multiple effectors. *Curr. Mol. Pharm.* **2**, 237–248 (2009).
- Nasman, J., Kukkonen, J. P., Ammoun, S. & Akerman, K. E. Role of G-protein availability in differential signaling by alpha 2-adrenoceptors. *Biochem Pharm.* **62**, 913–922 (2001).
- Xiao, R. P. Beta-adrenergic signaling in the heart: dual coupling of the beta2-adrenergic receptor to G(s) and G(i) proteins. *Sci. STKE* **2001**, re15 (2001).
- Ayoub, M. A., Trinquet, E., Pflieger, K. D. & Pin, J. P. Differential association modes of the thrombin receptor PAR1 with Galphai1, Galpha12, and beta-arrestin 1. *FASEB J.* **24**, 3522–3535 (2010).
- Hamamoto, A., Kobayashi, Y. & Saito, Y. Identification of amino acids that are selectively involved in Gi/o activation by rat melanin-concentrating hormone receptor 1. *Cell Signal* **27**, 818–827 (2015).
- Harding, S. D. et al. The IUPHAR/BPS Guide to PHARMACOLOGY in 2018: updates and expansion to encompass the new guide to IMMUNOPHARMACOLOGY. *Nucleic Acids Res.* **46**, D1091–D1106 (2018).
- Inoue, A. et al. Illuminating G-protein-coupling selectivity of GPCRs. *Cell* **177**, 1933–1947.e1925 (2019).
- Liang, Y. L. et al. Phase-plate cryo-EM structure of a class B GPCR-G-protein complex. *Nature* **546**, 118–123 (2017).
- Carpenter, B., Nehme, R., Warne, T., Leslie, A. G. & Tate, C. G. Structure of the adenosine A(2A) receptor bound to an engineered G protein. *Nature* **536**, 104–107 (2016).
- Rasmussen, S. G. et al. Crystal structure of the beta2 adrenergic receptor-Gs protein complex. *Nature* **477**, 549–555 (2011).
- Maeda, S., Qu, Q., Robertson, M. J., Skiniotis, G. & Kobilka, B. K. Structures of the M1 and M2 muscarinic acetylcholine receptor/G-protein complexes. *Science* **364**, 552–557 (2019).
- Garcia-Nafria, J. & Tate, C. G. Cryo-EM structures of GPCRs coupled to Gs, Gi and Go. *Mol. Cell Endocrinol.* **488**, 1–13 (2019).
- Gulukhova, A. et al. Rules of engagement: GPCRs and G proteins. *ACS Pharmacol. Transl. Sci.* **1**, 73–83 (2018).
- Du, Y. et al. Assembly of a GPCR-G protein complex. *Cell* **177**, 1232–1242.e1211 (2019).
- Okashah, N. et al. Variable G protein determinants of GPCR coupling selectivity. *Proc. Natl Acad. Sci. USA* **116**, 12054–12059 (2019).
- Strohman, M. J. et al. Local membrane charge regulates beta2 adrenergic receptor coupling to Gi3. *Nat. Commun.* **10**, 2234 (2019).
- Casella, I., Ambrosio, C., Gro, M. C., Molinari, P. & Costa, T. Divergent agonist selectivity in activating beta1- and beta2-adrenoceptors for G-protein and arrestin coupling. *Biochem J.* **438**, 191–202 (2011).
- Griffin, M. T., Figueroa, K. W., Liller, S. & Ehler, F. J. Estimation of agonist activity at G protein-coupled receptors: analysis of M2 muscarinic receptor signaling through Gi/o, Gs, and G15. *J. Pharm. Exp. Ther.* **321**, 1193–1207 (2007).
- Peralta, E. G., Ashkenazi, A., Winslow, J. W., Ramachandran, J. & Capon, D. J. Differential regulation of PI hydrolysis and adenylyl cyclase by muscarinic receptor subtypes. *Nature* **334**, 434–437 (1988).
- Chung, K. Y. et al. Conformational changes in the G protein Gs induced by the beta2 adrenergic receptor. *Nature* **477**, 611–615 (2011).
- Westfield, G. H. et al. Structural flexibility of the G alpha s alpha-helical domain in the beta2-adrenoceptor Gs complex. *Proc. Natl Acad. Sci. USA* **108**, 16086–16091 (2011).
- Tontson, L., Babina, A., Vosumaa, T., Kopanchuk, S. & Rinke, A. Characterization of heterotrimeric nucleotide-depleted Galpha(i)-proteins by Bodipy-FL-GTPgammaS fluorescence anisotropy. *Arch. Biochem. Biophys.* **524**, 93–98 (2012).
- McEwen, D. P., Gee, K. R., Kang, H. C. & Neubig, R. R. Fluorescent BODIPY-GTP analogs: real-time measurement of nucleotide binding to G proteins. *Anal. Biochem.* **291**, 109–117 (2001).
- Preininger, A. M., Meiler, J. & Hamm, H. E. Conformational flexibility and structural dynamics in GPCR-mediated G protein activation: a perspective. *J. Mol. Biol.* **425**, 2288–2298 (2013).
- Hermans, E. Biochemical and pharmacological control of the multiplicity of coupling at G-protein-coupled receptors. *Pharm. Ther.* **99**, 25–44 (2003).
- Cordeaux, Y., Ijzerman, A. P. & Hill, S. J. Coupling of the human A1 adenosine receptor to different heterotrimeric G proteins: evidence for agonist-specific G protein activation. *Br. J. Pharm.* **143**, 705–714 (2004).
- Arai, K. et al. Differential requirement of G alpha12, G alpha13, G alphaq, and G beta gamma for endothelin-1-induced c-Jun NH2-terminal kinase and extracellular signal-regulated kinase activation. *Mol. Pharm.* **63**, 478–488 (2003).
- Flock, T. et al. Selectivity determinants of GPCR-G-protein binding. *Nature* **545**, 317–322 (2017).
- Conklin, B. R., Farfel, Z., Lustig, K. D., Julius, D. & Bourne, H. R. Substitution of three amino acids switches receptor specificity of Gq alpha to that of Gi alpha. *Nature* **363**, 274–276 (1993).
- Hamm, H. E. et al. Site of G protein binding to rhodopsin mapped with synthetic peptides from the alpha subunit. *Science* **241**, 832–835 (1988).
- Rose, A. S. et al. Position of transmembrane helix 6 determines receptor G protein coupling specificity. *J. Am. Chem. Soc.* **136**, 11244–11247 (2014).
- Sandhu, M. et al. Conformational plasticity of the intracellular cavity of GPCR-G-protein complexes leads to G-protein promiscuity and selectivity. *Proc. Natl Acad. Sci. USA* **116**, 11956–11965 (2019).
- Natochin, M., Muradov, K. G., McEntaffer, R. L. & Artemyev, N. O. Rhodopsin recognition by mutant G(s)alpha containing C-terminal residues of transducin. *J. Biol. Chem.* **275**, 2669–2675 (2000).
- Semack, A., Sandhu, M., Malik, R. U., Vaidehi, N. & Sivaramakrishnan, S. Structural elements in the Galphas and Galphaq C termini that mediate selective G protein-coupled receptor (GPCR) signaling. *J. Biol. Chem.* **291**, 17929–17940 (2016).
- Yano, A. et al. An aromatic amino acid within intracellular loop 2 of the prostaglandin EP2 receptor is a prerequisite for selective association and activation of Galphas. *Biochim Biophys. Acta Mol. Cell Biol. Lipids* **1862**, 615–622 (2017).
- Masson, G. R. et al. Recommendations for performing, interpreting and reporting hydrogen deuterium exchange mass spectrometry (HDX-MS) experiments. *Nat. Methods* **16**, 595–602 (2019).
- Deutsch, E. W. et al. The ProteomeXchange consortium in 2020: enabling 'big data' approaches in proteomics. *Nucleic Acids Res.* **48**, D1145–D1152 (2020).
- Perez-Riverol, Y. et al. The PRIDE database and related tools and resources in 2019: improving support for quantification data. *Nucleic Acids Res.* **47**, D442–D450 (2019).

Acknowledgements

This work was supported by the National Research Foundation of Korea funded by the Korean government (NFR-2018R1A2B6001554 and NRF-2019R1A5A2027340) (K.Y.C.) and funds from Kobilka Institute of Innovative Drug Discovery by the Science and Technology Innovation Committee of Shenzhen (Y.D.). The authors thank Dr. Brian K. Kobilka for valuable discussion.

Author contributions

Y.D., J.X., and S.M. purified the β_2 AR, M2R, Gi3, and GoA proteins. Y.D. and J.X. performed GDP release assay, generated mutant constructs, and wrote the manuscript. H.R.K. prepared GPCR-Gi/o complexes, performed HDX-MS and BODIPY-GTP γ S assays, analyzed mass spectrometry data, and generated mutant constructs. N.M.D. analyzed mass spectrometry data. D.A. prepared Gi3 mutant construct. Y.D. and K.Y.C. initiated the project, supervised research, analyzed data, and wrote the manuscript with contributions from all authors.

Competing interests

The authors declare no competing interests.

Additional information

Supplementary information is available for this paper at <https://doi.org/10.1038/s41467-020-16975-2>.

Correspondence and requests for materials should be addressed to Y.D. or K.Y.C.

Peer review information *Nature Communications* thanks John Burke and the other, anonymous, reviewer(s) for their contribution to the peer review of this work.

Reprints and permission information is available at <http://www.nature.com/reprints>

Publisher's note Springer Nature remains neutral with regard to jurisdictional claims in published maps and institutional affiliations.



Open Access This article is licensed under a Creative Commons Attribution 4.0 International License, which permits use, sharing, adaptation, distribution and reproduction in any medium or format, as long as you give appropriate credit to the original author(s) and the source, provide a link to the Creative Commons license, and indicate if changes were made. The images or other third party material in this article are included in the article's Creative Commons license, unless indicated otherwise in a credit line to the material. If material is not included in the article's Creative Commons license and your intended use is not permitted by statutory regulation or exceeds the permitted use, you will need to obtain permission directly from the copyright holder. To view a copy of this license, visit <http://creativecommons.org/licenses/by/4.0/>.

© The Author(s) 2020